# Conformational and NMR study of some furan derivatives by DFT methods

**ARTICLE** *in* JOURNAL OF MOLECULAR MODELING · JULY 2013

Impact Factor: 1.74 · DOI: 10.1007/s00894-013-1964-z · Source: PubMed



**5 AUTHORS**, INCLUDING:

David Santos-Carballal
University College London
**6** PUBLICATIONS **22** CITATIONS
SEE PROFILE

Reynier Suardiaz
King's College London
**33** PUBLICATIONS **167** CITATIONS
SEE PROFILE

Rachel Crespo
Queen Mary, University of London
**52** PUBLICATIONS **421** CITATIONS
SEE PROFILE

Carlos S. Pérez
University of Havana
**71** PUBLICATIONS **436** CITATIONS
SEE PROFILE

J Mol Model (2013) 19:4591–4601
DOI 10.1007/s00894-013-1964-z

ORIGINAL PAPER

# Conformational and NMR study of some furan derivatives by DFT methods

**David Santos-Carballal · Reynier Suardíaz · Rachel Crespo-Otero · Leandro González · Carlos S. Pérez**

Received: 3 May 2013 / Accepted: 25 July 2013 / Published online: 22 August 2013


**Abstract** 4′-substituted neutral/protonated furfurylidenanilines and trans-styrylfurans are able to exist in two different conformations related to the rotation around the furan ring-bridge double bond. In this work, the equilibrium geometry and the corresponding rotational barrier of the benzene ring for each furan derivative conformation were calculated by DFT methods. The trend and shape of the rotational barrier are rationalized within natural bond orbitals as well as atoms-in-molecules approach. For the corresponding equilibrium geometries, $^{1}H$ and $^{13}C$ substituent induced shifts (SIS) were calculated and compared with experimental values. Calculated shielding constants are shown to be sensitive to the substituent effect through a linear fit with substituent's Hammett constants. An alternative approach was followed for assessing the effect of substituents over SIS through comparing the differences in isotropic shielding constants with NBO charges as well as with $^{1}H$ and $^{13}C$ experimental chemical shifts.

**Keywords** Chemical shifts · Furfurylidenanilines · Rotational barriers · Styrylfurans

**Electronic supplementary material** The online version of this article (doi:10.1007/s00894-013-1964-z) contains supplementary material, which is available to authorized users.

D. Santos-Carballal · R. Suardíaz · R. Crespo-Otero · L. González · C. S. Pérez (✉)
Departamento de Química Física, Facultad de Química, Universidad de La Habana, Ciudad de La Habana, Cuba
e-mail: cp@fq.uh.cu

*Present Address:*
D. Santos-Carballal
Department of Chemistry, University College London, 20 Gordon Street, London WC1H 0AJ, UK

*Present Address:*
R. Suardíaz (✉)
Department de Química and Institut de Biotecnologia i de Biomedicina (IBB), Universitat Autònoma de Barcelona, Bellaterra, 08193 Barcelona, Spain
e-mail: reynier.suardiaz@gmail.com

*Present Address:*
R. Crespo-Otero
Max-Planck-Institut für Kohlenforschung, Kaiser-Wilhelm-Platz 1, 45470 Muelheim an der Ruhr, Germany

*Present Address:*
L. González
Departamento de Investigación, Centro Nacional del Hidrógeno 2, Ciudad Real, Spain

## Introduction

Quantum mechanical calculations of nuclear magnetic resonance (NMR) parameters are nowadays routine in computational chemistry [1–12]. Their applications ranges from organic [13–18] and inorganic [19, 20] chemistry to biomolecules [8, 11, 21–24] and solid state [25–29]. The well-known and most studied NMR parameters, $^{1}H$ and $^{13}C$ chemical shifts, have been widely used for predicting molecular structures or to distinguish between some substrates using established databases of correlated chemical shifts [30]. Sometimes this correlation cannot be found experimentally and should be computed [30]. However, this requires the estimation of many local and remote factors, usually long time consuming. An alternative implementation of expensive computational methods is density functional theory (DFT) due to its convenient ratio results-quality/computational-cost [12]. Moreover, it has become the conventional and almost trouble-free method for calculating shielding tensors for simple and diverse molecules with light atoms [12, 31–33].

N-(4′-substituted-phenyl)-2-furaldimines, Fig. 1 (FA when Y=N), are important intermediates in the synthesis of their corresponding aminoalkyl pyridines [34–36], $\Delta^2$-1,2,3-triazolines (4,5-dihydro-1H-1,2,3-triazoles) and 1H-1,2,3-triazoles which show remarkable pharmacological activity as anticonvulsants [37, 38]. These aromatic azomethines are

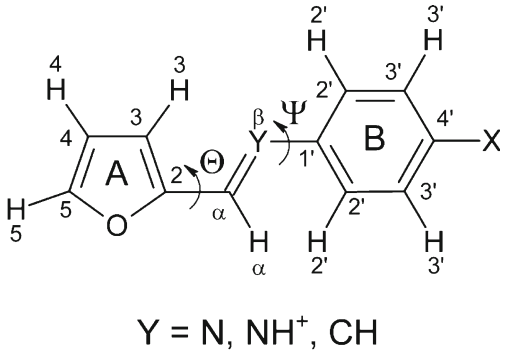


**Fig. 1** United representation of neutral/protonated FA and trans-SF (X: $NO_2$, CN, F, Cl, Br, H, $CH_3$, $OCH_3$, OH, $NH_2$, $N(CH_3)_2$)

easily obtained by direct reaction of furfural with aniline derivatives [39].

Neutral and protonated FA exist mainly as E isomer (defined by rotation around $C_\alpha$=Y double bond) at room temperature [40, 41]. Among the most notable evidence is the $^1JC_\alpha H_\alpha$=161.6 Hz measured by Pérez [42], which suggests the existence of E structure only [40]. This is supported by the experimental $^3JH_\alpha H_N$=17 Hz [42–44], which denotes the preference of protonated azomethines, including protonated FA, to exist as E isomer. Furthermore, the interconversion of neutral FA from Z to E isomer is fast due to the nitrogen inversion [45–47].

This work presents the DFT calculation of Ψ rotational barriers of neutral and protonated furfurylidenanilines (FA, Y=N, $NH^+$) and their non-polar analogues trans-styrylfurans (SF, Y=CH), Fig. 1, which are rationalized in terms of natural bond orbital (NBO) and atoms-in-molecules (AIM) electronic localization schemes. Additionally, in this study we report the DFT estimation of $^1$H and $^{13}$C isotropic magnetic shielding constants (σ) and make an analysis of the 4′-substituent electronic influence on them.

## Computational section

Full geometry optimizations were performed for all 4′-substituted compounds using DFT-B3LYP [48–51] functional in combination with 6-31G(d,p) basis set. We carried out constrained geometry calculations for 12 rotations in all furan derivatives around Ψ dihedral angle starting at 0° and finishing at 165°, while the rest of the variables were allowed to relax. Additionally, the transition states (TS) and equilibrium geometries of these molecules for such rotations around Ψ angle were calculated. These stationary points were fully optimized and characterized with frequency calculations. This methodology was applied to OY-syn (Θ dihedral angle of 0°) and OY-anti (Θ dihedral angle of 180°) conformers. For neutral/protonated FA only the stable E isomers were modeled.

Calculations of the trace of the shielding tensor (σ) for the corresponding equilibrium geometries were carried out within GIAO [52] methodology using DFT-B3LYP [48, 49] functional with 6-311G(d,p) basis set. NBO [53] and AIM analysis were performed at the same level of theory of geometry optimizations.

Geometry optimizations, shielding tensors as well as NBO calculations of the furan derivatives were carried out using Gaussian03 package of programs [54]. The calculation of AIM critical points were performed using EXTREME code and the atomic basins integrations were performed using PROAIM code, both in AIMPAC package [55]. The contour plot of the electronic density (Fig. S1 in supporting information) was created using AIM2000 program [56].

## Results and discussion

### Rotational barriers and equilibrium geometries

Our calculations show that Θ dihedral angle for the equilibrium geometry is almost 0° for OY-syn conformers and approximately equal to 180° for OY-anti conformers. Consequently, ring A and $C_\alpha$=Y double bond are coplanar in the equilibrium geometries of trans-SF as well as of neutral and protonated FA. However, the effect of the rotation of Ψ angle is more complicated. For the equilibrium geometry of some furfural derivatives, it is found that the whole molecule is planar, while in others, ring B is lying out of the plane of the rest of the molecule.

The calculations performed using DFT (B3LYP/6-31G(d,p)) of trans-SF equilibrium geometries show that OC-syn and OC-anti conformers are planar molecules. Ψ dihedral angle in the equilibrium geometry is 0° and the corresponding rotational barrier is not sensitive to the substituent effect and very similar for both conformers, with values around 6 kcal $mol^{-1}$, Fig. 2(a) and (b). The planarity of the trans-SF derivatives is supported by the planarity in solid phase (X-ray diffraction [57]) and near planarity in the gas phase (electronic diffraction) [58] of trans-stilbene, the non-heterocyclic analogue of trans-SF.

Likewise, the equilibrium geometries of ON-syn and ON-anti conformers of protonated FA derivatives are essentially planar, Fig. 2(c) and (d). The minima around Ψ=0° are very shallow and the plateaus are slightly more marked in ON-anti conformers. The calculated rotational barriers, of both protonated FA conformers, are relatively insensitive to the electronic effect of substituents.

Unlike the previously presented furan derivatives, the equilibrium geometries of both conformers of neutral FA are non-planar, as shown in Table S3 (in supporting information). Therefore, this non-planarity leads to two rotational barriers in neutral FA, one through Ψ=0° and other through Ψ=90°, Fig. 2(e) and (f).

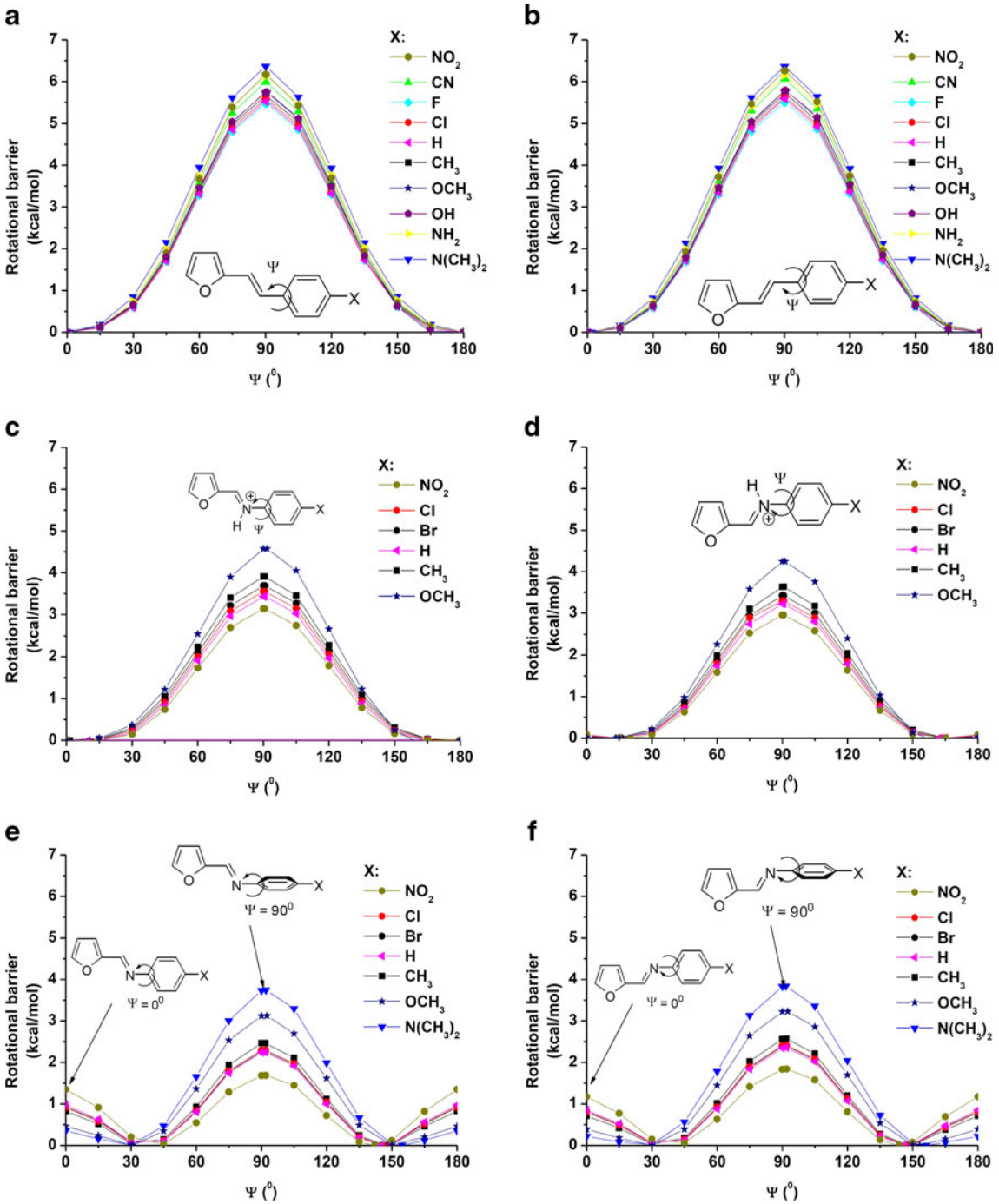


**Fig. 2** Rotational barriers of trans-SF derivatives (**a**) OC-syn and (**b**) OC-anti conformations; protonated FA derivatives (**c**) ON-syn and (**d**) ON-anti conformations; and neutral FA derivatives (**e**) ON-syn and (**f**) ON-anti conformations

Both rotational barriers of ON-syn and ON-anti conformers of neutral FA are very similar and sensitive to substituent effects, especially the highest barrier, which is through Ψ=90°, as can be seen in Fig. 2(e) and (f). The shape of the rotational barriers curves as well as the Ψ dihedral angle of the equilibrium geometry of neutral FA derivatives seem to depend strongly on the mesomeric effect of the 4′-substituent. The height of their rotational barrier curves in Ψ=90° increases with electron donor substituents. On the other hand, the height of the rotational barrier in Ψ=0°, together with Ψ angle values of the equilibrium geometry in neutral FA, decrease with the same type of substituent. Various investigations of the molecular structure of N-benzylideneanilines [59–61] have shown that electronic effects of substituents in ring B can largely influence the equilibrium value of Ψ dihedral angle and then determine the non-planar molecular conformation.

As the employed functional, B3LYP, is local in correlation and there is significant stabilization by π=>π* as demonstrated

later; we have performed additional calculations with the dispersion-corrected functional M06 and B3LYP-D of neutral FA derivatives rotational barriers. The inclusion of the dispersion correction slightly modifies the value of the barriers heights. M06 produces larger rotational barriers than B3LYP both at 0° and 90° while the rotational barriers derived from B3LYP-D are larger than with B3LYP at 90° and smaller than with B3LYP at 0°. Nevertheless, the inclusion of dispersion correction in the functionals does not affect the energy ordering of the substituents in neutral FA (see Table S4 in supporting information for details).

For all furan derivatives, the order for the rotational barrier height range of values is trans-SF>protonated FA>neutral FA, while the order for the Ψ dihedral angle range of values of the equilibrium geometry is neutral FA>protonated FA>trans-SF.

The traditional explanation for the non-planarity of neutral FA takes into account the competition between two principal factors: (1) steric interaction between $H_{2'}$ and $H_{\alpha}$, which is repulsive in the planar conformation but is reduced with increasing non-planarity and (2) conjugation effects, divisible into two components, π delocalization between azomethine double bond and the ring B, which is maximized for planar conformations, and, on the other hand, delocalization of the nitrogen lone pair electrons with ring B π system which is absent in the planar conformation but increases with increasing non-planarity [62]. An AIM and NBO analysis is carried out in the next section to analyze the principal factors that determine the rotational barrier of neutral FA.

## NBO and AIM analysis of neutral FA

In order to estimate the conjugation effects governing the rotational barriers of neutral FA, we carried out an NBO analysis [63] using DFT: B3LYP/6-31G(d,p). According to the donor–acceptor scheme the strongest electronic interactions between ring B and $C_{\alpha}$=N double bond are π ($C_{\alpha}$-N) =>π*($C_{1'}$-$C_{2'}$) and π ($C_{1'}$-$C_{2'}$) =>π*($C_{\alpha}$-N) that stabilize the planar geometry (Ψ=0°) as well as LP (N) =>π*($C_{1'}$-$C_{2'}$) which stabilizes the geometry with orthogonal π moieties (Ψ=90°). Table 1 lists the values of π-π and LP-π donor-acceptor components as well as the total effect of them in both conformers of 4′-substituted neutral FA when Ψ=0° and 90°.

As we can see in Table 1, the net conjugation effect stabilizes the planar geometry more than the perpendicular. Moreover, LP (N) =>π*($C_{1'}$-$C_{2'}$) is strongly sensitive to the electronic substituent effect. Consequently, this type of electronic interaction probably accounts for the change of Ψ angle values in the equilibrium geometries of 4′-substituted neutral FA and the change of their energy barriers (through Ψ=90°).

On the other hand, the net contribution of the conjugative interactions that stabilize the planar conformation is rather non-sensitive to the substituents electronic effects. This results from opposed tendencies of π ($C_{\alpha}$-N) =>π*($C_{1'}$-$C_{2'}$) and π ($C_{1'}$-$C_{2'}$) =>π*($C_{\alpha}$-N). We present below an AIM approach for accounting the instabilities of the planar structures of 4′-substituted neutral FA.

**Table 1** Donor-acceptor scheme second order correction energies (kcal $mol^{-1}$) of neutral FA

| X | Conformer | TS (0°) | | | TS (90°) |
|---|---|---|---|---|---|
| | | π ($C_{\alpha}$-N) ↓ π ($C_{1'}$-$C_{2'}$)* | π ($C_{1'}$-$C_{2'}$) ↓ π ($C_{\alpha}$-N)* | Total | LP (N) ↓ π ($C_{1'}$-$C_{2'}$)* |
| $NO_2$ | ON-syn | 15.47 | 14.79 | 30.26 | 16.57 |
| Cl | | 14.20 | 15.62 | 29.82 | 14.28 |
| Br | | 14.17 | 15.58 | 29.75 | 14.06 |
| H | | 13.82 | 15.82 | 29.64 | 14.00 |
| $CH_3$ | | 13.67 | 16.14 | 29.81 | 13.65 |
| $OCH_3$ | | 13.51 | 16.84 | 30.35 | 13.09 |
| $N(CH_3)_2$ | | 13.15 | 17.76 | 30.91 | 12.51 |
| $NO_2$ | ON-anti | 15.64 | 14.60 | 30.24 | 16.24 |
| Cl | | 14.31 | 15.38 | 29.69 | 14.04 |
| Br | | 14.20 | 15.54 | 29.74 | 14.32 |
| H | | 13.96 | 15.62 | 29.58 | 13.77 |
| $CH_3$ | | 13.81 | 15.92 | 29.73 | 13.44 |
| $OCH_3$ | | 13.64 | 16.61 | 30.25 | 12.88 |
| $N(CH_3)_2$ | | 13.27 | 17.55 | 30.82 | 12.39 |

A destabilizing factor of the planar conformation in neutral FA is the steric repulsion between $H_{\alpha}$ and $H_{2'}$, analogous to the repulsion present in biphenyls. Nevertheless, Bader et al. [64, 65] in their atom-in-molecules theory (AIM) [66] found that this kind of H···H interaction in biphenyl systems contributes to the system stabilization, being both hydrogen atoms linked by a bond path, and that the destabilization of the planar structures is related to the lengthening of the C-C bond between biphenyl moieties. A set of C-H···H-C interactions have been characterized using their experimental electron densities and the AIM methodology [67], supporting Bader assumptions. However, a work of Sola et al. [68–69] attributes the planar conformation destabilization in biphenyls to the Pauli repulsion between molecular orbitals ($C_{ortho}$-$H_{ortho}$) and rejects the hypothesis of H···H bonding stabilization.

An analysis of the interaction that involves $H_{\alpha}$ and $H_{2'}$ atoms in the planar structures of all neutral FA derivatives was carried out within AIM framework using DFT: B3LYP/6-31G(d,p). EXTREME program included in AIMPAC package [55] was the code used for all AIM calculations.

AIM provides valuable information of the molecular structure based on the analysis of electron densities. On these grounds, the critical points and the Laplacian of the electron densities are analyzed and characterized. The number of non-zero eigenvalues of the Hessian matrix on a critical point defines its rank (σ) and the sum of the signs of these eigenvalues its signature (λ). The (σ, λ) code is used to characterize

a critical point. If a pair of atoms are bonded, there is a path of maximum charge density between them, with a saddle point along the path. This line is called bond path (bp) and the saddle point a bond critical point (bcp). In a bcp, the electron density has a maximum in two directions and a minimum in the third perpendicular direction. A bcp is described with the code: (3,-1). $\lambda_1$, $\lambda_2$ and $\lambda_3$ are the curvatures or eigenvalues of the Hessian matrix of the electron density. A useful parameter is the ellipticity ($\varepsilon=\lambda_1/\lambda_2-1$) of the electron density at the bond critical points. It provides a quantitative description of the anisotropy of the electron density at the bcp.

We found one (3,-1) bond critical point (bcp), which has topological features similar to usual closed shell interactions, between each pair of $H_\alpha\cdots H_{2'}$ in both conformations of all neutral FA derivatives. In line with AIM theory, a bcp is one of the factors determining the distance between the atoms that it joins (in this case $H_\alpha\cdots H_{2'}$ distance) and therefore influencing the stability of the planar conformations of neutral FA.

For the set of studied derivatives the distance ($r$) between $H_\alpha\cdots H_{2'}$ was found to be between 2.052–2.085 Å for ON-syn and 2.054–2.089 Å for ON-anti conformers, Table 2. Although this variation of $H_\alpha\cdots H_{2'}$ distance is small, the electronic density ($\rho(r_c)$) in the interatomic region decreases slightly and lineally with the increment of the distance between $H_\alpha\cdots H_{2'}$. We found that such $\rho(r_c)$ are small for all bcps and they deplete locally in the bcp, where the local excess of kinetic energy is dominant over the potential energy, which explains the weakness of $H_\alpha\cdots H_{2'}$ interactions and the small values of the electronic density Laplacian $\nabla^2\rho(r_c)>0$. Moreover, we calculated $\lambda_3$ (*eigen*value of the Hessian matrix) for the bcps, for which positive values agree with the expected minimum along the bond path for the charge density. On the other hand, the associated curvatures ($\lambda_1$ and $\lambda_2$) of the charge density in the interatomic surface, which are negative and perpendicular to the bond path Table 2, attain their maximum value in the bcp, suggesting some stabilizing interaction between $H_\alpha\cdots H_{2'}$.

All considered bcp's have ellipticities close to 1 which mean asymmetrically distributed electron densities. We found the same trend in all bcp between $H_\alpha\cdots H_{2'}$ in both conformations of 4′-substituted neutral FA, Table 2.

For non-substituted neutral FA we carried out a more detailed study in order to understand the origin of the rotational barrier through $\Psi=0°$. Integration over atomic basins were calculated to obtain the atomic properties using PROAIM program [55].

We found that atomic energies decrease 4.14 kcal mol$^{-1}$ and 3.01 kcal mol$^{-1}$ for $H_\alpha$ and $H_{2'}$ respectively in ON-syn conformer (2.21 kcal mol$^{-1}$ and 2.93 kcal mol$^{-1}$ for $H_\alpha$ and $H_{2'}$ respectively in ON-anti conformer), due to the stabilizing effects related to the formation of the bcp. At the same time, the energy of the bond N-$C_{1'}$ increases and it adds 15.91 kcal mol$^{-1}$ to the total energy in ON-syn conformer (23.38 kcal mol$^{-1}$ in ON-anti conformer). Consequently, the distance of N-$C_{1'}$ bond increases in the transition from the twisted minima to the planar form, which reflects the instability of the latter and it is in agreement with reports for biphenyl systems [64, 65]. Therefore, according to AIM theory the origin of the barrier through $\Psi=0°$ is related to the instability of the bond N-$C_{1'}$ that is forced by the formation of a bcp between $H_\alpha\cdots H_{2'}$.

Among all properties presented here related to the bcps studied, the most affected variable in neutral FA by substitution is $\nabla^2\rho(r_c)$. Thus, the stability of the bcp's can be associated with the energy barrier between the minimum and the

**Table 2** Features of the bcp between $H_\alpha\cdots H_{2'}$ in 4′-substituted neutral FA

| X | Conformers | $r$ (H-H) (Å) | $\rho(r_c)$ (e/au$^3$) | $\nabla^2\rho(r_c)$ (e/au$^5$) | $\lambda_1$ (e/au$^5$) | $\lambda_2$ (e/au$^5$) | $\lambda_3$ (e/au$^5$) | $\varepsilon=\frac{\lambda_1}{\lambda_2}-1$ |
|---|---|---|---|---|---|---|---|---|
| $NO_2$ | ON-syn | 2.052 | 0.01156 | 0.04926 | −0.01217 | −0.00611 | 0.06754 | 0.9917 |
| Cl | | 2.064 | 0.01131 | 0.04811 | −0.01181 | −0.00588 | 0.06580 | 1.0100 |
| Br | | 2.063 | 0.01135 | 0.04822 | −0.01186 | −0.00591 | 0.06599 | 1.0067 |
| H | | 2.057 | 0.01151 | 0.04850 | −0.01208 | −0.00625 | 0.06683 | 0.9328 |
| $CH_3$ | | 2.065 | 0.01135 | 0.04791 | −0.01184 | −0.00599 | 0.06574 | 0.9762 |
| $OCH_3$ | | 2.072 | 0.01118 | 0.04742 | −0.01162 | −0.00576 | 0.06479 | 1.0161 |
| $N(CH_3)_2$ | | 2.085 | 0.01094 | 0.04643 | −0.01125 | −0.00541 | 0.06309 | 1.0809 |
| $NO_2$ | ON-anti | 2.054 | 0.01156 | 0.04934 | −0.01214 | −0.00596 | 0.06743 | 1.0379 |
| Cl | | 2.066 | 0.01131 | 0.04817 | −0.01178 | −0.00572 | 0.06567 | 1.0587 |
| Br | | 2.065 | 0.01133 | 0.04824 | −0.01180 | −0.00573 | 0.06578 | 1.0588 |
| H | | 2.060 | 0.01147 | 0.04847 | −0.01200 | −0.00603 | 0.06650 | 0.9870 |
| $CH_3$ | | 2.067 | 0.01135 | 0.04800 | −0.01181 | −0.00584 | 0.06566 | 1.0209 |
| $OCH_3$ | | 2.074 | 0.01120 | 0.04742 | −0.01164 | −0.00580 | 0.06450 | 1.0070 |
| $N(CH_3)_2$ | | 2.089 | 0.01091 | 0.04640 | −0.01117 | −0.00520 | 0.06278 | 1.1480 |

planar transition state using $\nabla^2\rho(r_c)$, for which correlation coefficient is 0.969 for ON-syn conformer (0.999 for ON-anti conformer). Therefore, all these results suggest that the bcp between $H_{\alpha}\cdots H_{2'}$ plays an important role in the transition state stabilization according to AIM theory.

## NMR analysis

### *Calculation and analysis of $^{13}C$ chemical shifts*

$^{13}C$ shielding tensors ($\sigma^{13}C$) of the equilibrium geometries of trans SF as well as neutral and protonated FA derivatives were calculated using DFT: B3LYP/6-311G(d,p). The reliability of calculated $\sigma^{13}C$ values was verified by fitting them to experimental chemical shifts ($\delta^{13}C$) [42], Eq. 1. In this way, the intercept of the fitting line with $\sigma^{13}C_{calc}$ axis, Eq. 2, is isotropic shielding constant of the reference ($\sigma^{13}C_{ref}$), which includes the dispersion of the calculated $\sigma^{13}C$ with respect to the experimental $\delta^{13}C$. Therefore, in this work $\sigma^{13}C_{ref}$ is used as a unique parameter to measure the accuracy of the calculations by comparing it with the ideal $\sigma^{13}C$ calculated for the reference (tetramethylsilane, TMS).

$$\delta^{13}C_{exp} = a + b\cdot\sigma^{13}C_{calc} \quad (1)$$

$$-\frac{a}{b} = \sigma^{13}C_{ref} \quad (2)$$

Table 3 shows $\sigma^{13}C_{ref}$ of TMS calculated using DFT as well as obtained according to Eq. 2 for all furan derivatives studied.

It is possible to see in Table 3 the good quality of the calculations; because of the good agreement between $\sigma^{13}C_{ref}$ obtained using Eq. 2 for the reference of both conformers of trans-SF and neutral FA derivatives as well as $\sigma^{13}C_{ref}$ of TMS calculated using DFT. On the other hand, $\sigma^{13}C$ of protonated FA derivatives are the poorest reproduced by DFT calculations, probably due to not considering the solvent effect in the modeling [70]. Alternatively, the reliability of DFT calculations of $\sigma^{13}C_{ref}$ for all furan derivatives is illustrated graphically in Fig. S2 (supporting information).

**Table 3** Linear fit of experimental $\delta^{13}C$ vs. calculated $\sigma^{13}C$ in ppm

| Molecules | $\sigma^{13}C_{ref}$ | Calculation method |
|---|---|---|
| TMS | 184.31 | GIAO, DFT: B3LYP/6–311G(d,p) |
| Trans-SF OC-syn | 186.08 | $\delta^{13}C_{exp} = a + b\cdot\sigma^{13}C_{calc}$ |
| Trans-SF OC-anti | 191.61 | $-\frac{a}{b} = \sigma^{13}C_{ref}$ |
| Protonated FA ON–syn | 203.59 | |
| Protonated FA ON–anti | 208.08 | |
| Neutral FA ON–syn | 184.68 | |
| Neutral FA ON–anti | 192.11 | |

Tables S5–S10 (in supporting information) show $\sigma^{13}C$ calculated for all furfural derivatives. Clearly, the effect of increasing the electron-donor properties of the substituent in 4′ promotes a change of $\sigma^{13}C$, which is more marked in certain positions of the furan derivatives. Specifically, the alternating carbon atoms labeled as 1′, α, 3 and 5, all of which are in conjugative positions, have the most affected $\sigma^{13}C$ by the electronic effect of substituents. Conversely, carbon atoms occupying non-conjugative positions, such as β, 2 and 4 are much less affected by substitution. Therefore, with the aim of assessing quantitatively the substituent effect in $\sigma^{13}C$, we use the Hammett equation, Eq. 3.

$$\sigma^{13}C(\text{ppm}) = a + b\cdot\sigma_p(-X) \quad (3)$$

where $\sigma_p$ [71, 72] is the Hammett constant of each 4′ substituent (−X).

Table 4 lists the correlation parameters of the Hammett equation for all furan derivatives, where $R$ is the correlation coefficient.

**Table 4** Hammett coefficients for $^{13}C$-SIS

| | | 1′ | β | α | 2 | 3 | 4 | 5 |
|---|---|---|---|---|---|---|---|---|
| Trans-SF OC-syn | *a* | 43.3 | 52.1 | 64.5 | 22.6 | 68.5 | 66.5 | 35.7 |
| | *b* | −11.0 | 2.0 | −5.8 | 1.2 | −4.2 | −0.8 | −2.4 |
| | *R* | 0.91 | 0.78 | 0.98 | 0.99 | 0.98 | 0.94 | 0.98 |
| Trans-SF OC-anti | *a* | 43.3 | 52.6 | 62.1 | 21.2 | 73.5 | 66.1 | 36.6 |
| | *b* | −11.0 | 2.1 | −6.1 | 1.3 | −3.8 | −0.8 | −2.6 |
| | *R* | 0.91 | 0.78 | 0.98 | 0.98 | 0.97 | 0.94 | 0.97 |
| Protonated FA ON-syn | *a* | 48.0 | | 45.4 | 33.6 | 40.8 | 57.8 | 16.7 |
| | *b* | −9.0 | | −5.0 | 0.2 | −6.0 | −1.7 | −4.0 |
| | *R* | 0.62 | | 0.67 | 0.31 | 0.84 | 0.93 | 0.89 |
| Protonated FA ON-anti | *a* | 47.0 | | 40.4 | 32.4 | 50.5 | 57.5 | 14.9 |
| | *b* | −9.0 | | −5.0 | 0.2 | −4.9 | −1.8 | −4.3 |
| | *R* | 0.62 | | 0.67 | 0.14 | 0.84 | 0.94 | 0.89 |
| Neutral FA ON-syn | *a* | 26.7 | | 35.9 | 22.8 | 60.5 | 66.7 | 32.0 |
| | *b* | −11.0 | | −5.0 | 1.1 | −3.8 | −0.7 | −2.2 |
| | *R* | 0.86 | | 0.91 | 0.99 | 0.99 | 0.93 | 0.98 |
| Neutral FA ON-anti | *a* | 27.0 | | 32.9 | 21.2 | 66.1 | 65.6 | 32.9 |
| | *b* | −11.0 | | −5.5 | 1.0 | −3.6 | −0.7 | −2.5 |
| | *R* | 0.86 | | 0.91 | 0.97 | 0.98 | 0.92 | 0.98 |

The slope (sign and value) of the line defined by the Hammett equation is a convenient measure for quantifying the magnitude of the substituent induced shift (SIS) in $^{13}C$. This means that increasing the electron donor effect of substituents in 4′ induces an up-field shift of $^{13}C$ SIS in conjugative positions and hence the sign of the resulting slope is negative, while the opposite and weaker effect is found in non-conjugative positions. Moreover, SIS decrease in remote positions of the substituent, which is reflected with the smaller absolute value of the slope in Eq. 3. Consequently, the order in the sensitivity of the $^{13}C$ SIS to the electronic effect of substituents in 4′ is:

$$|b_{1'}| > |b_{\alpha}| > |b_3| > |b_5| > |b_4|.$$

Our calculations show that the $C_{\alpha}=C_{\beta}$ double bond in trans-SF is a very efficient link for transmitting the effect of the substituent in 4′ to carbon atoms in ring A. Conversely, the $C_{\alpha}=N$ double bond in neutral FA is the least efficient link according to Hammett equation results.

SIS can be computationally modeled as isotropic shielding constant ($\Delta\sigma_{calc}$) variations and experimentally as chemical shift ($\Delta\delta_{exp}$) differences in the same carbon atom of two furan derivatives with the most electron-donor and most electron-withdrawing substituent in 4′. Furthermore, as $^{13}C$ SIS ($\Delta\delta_{exp}$) depends mainly on local paramagnetic currents, which are related to local electronic charges ($q$), $\Delta\delta_{exp}$ can be correlated with local electronic charge variations ($\Delta q$). Therefore, in this study SIS are modeled in three different ways, as $\Delta\sigma_{calc}$, $\Delta\delta_{exp}$ and $\Delta q$.

The experimental trends in $^{13}C$–SIS for all systems are well reproduced by both calculated isotropic shielding differences and NBO charge variations, Fig. 3 and Fig. S6. We only show ON-syn conformation because of the similarity of the experimental and calculated chemical shifts as well as of the NBO charges in the two conformations studied. However, trends of calculated shieldings are only slightly better than trends of NBO charges in the reproduction of the experimental data, which confirms the leading role of charge modifications in SIS.

### *Calculation and analysis of $^{1}H$ chemical shifts*

$^{1}H$ shielding tensors ($\sigma^{1}H$) were also calculated in this work for trans-SF and neutral/protonated FA derivatives.

The reliability of the calculated $\sigma^{1}H$ was assessed using the same method that was followed with $\sigma^{13}C$. In this manner, the intercept of Eq. 4 with $\sigma^{1}H$ axis, Eq. 5 which is the isotropic shielding of the reference ($\sigma^{1}H_{ref}$) was compared with $\sigma^{1}H$ calculated using DFT for TMS.

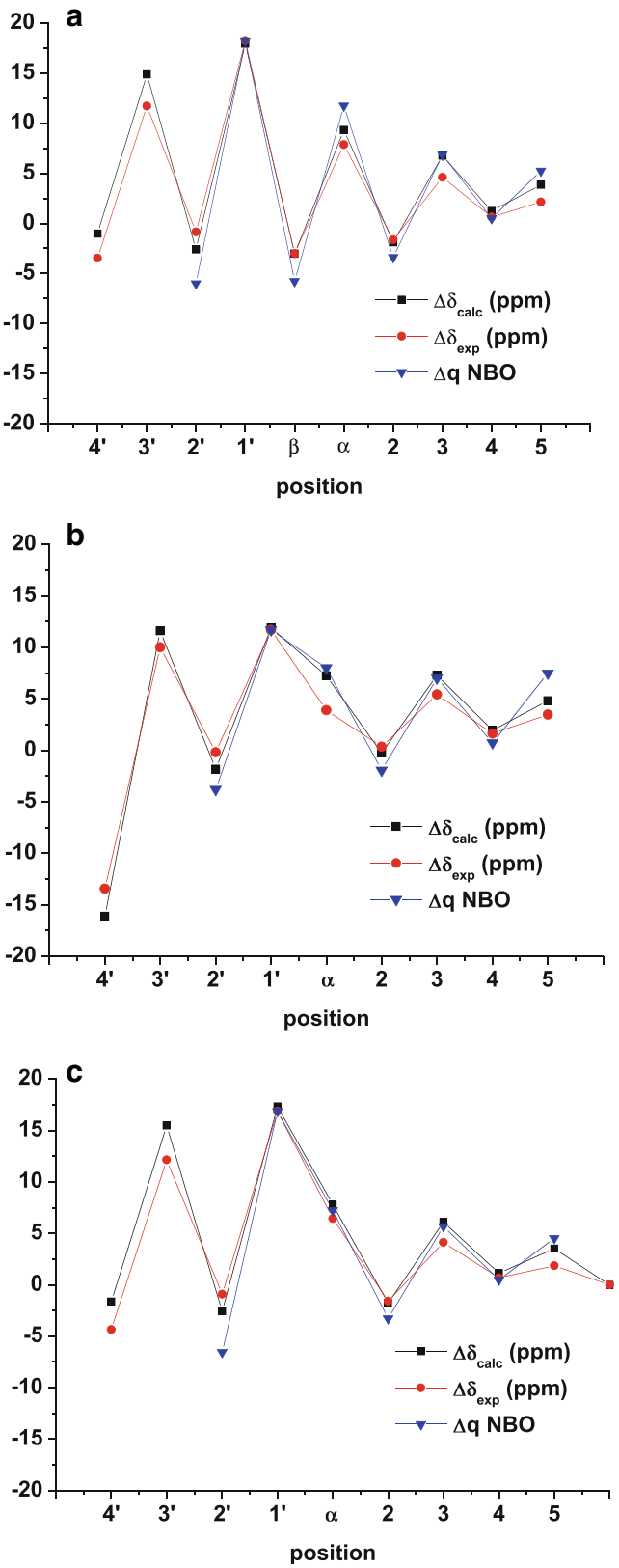


**Fig. 3** $^{13}C$ SIS transmission for (**a**) trans-SF OC-syn (**b**) protonated FA ON-syn and (**c**) neutral FA ON-syn. The $\Delta q$ were calibrated to $\Delta\delta_{exp}$ of position 1′

**Table 5** Linear fit of $\delta^1$H experimental vs. $\sigma^1$H calculated in ppm

| Molecules | $\sigma^1 H_{ref}$ | Calculation method |
|---|---|---|
| TMS | 31.95 | GIAO, DFT: B3LYP/6–311G(d,p) |
| Trans SF OC-syn | 32.45 | $\delta^1 H_{exp} = a + b{\cdot}\sigma^1 H_{calc}$ |
| Trans SF OC-anti | 31.70 | $-\frac{a}{b} = \sigma^1 H_{ref}$ |
| Protonated FA ON–syn | 31.28 | |
| Protonated FA ON–anti | 31.34 | |
| Neutral FA ON–syn | 32.21 | |
| Neutral FA ON–anti | 32.18 | |

$$\delta^1 H_{exp} = a + b{\cdot}\sigma^1 H_{calc} \quad (4)$$

$$-\frac{a}{b} = \sigma^1 H_{ref} \quad (5)$$

$\sigma^1 H_{ref}$ of TMS calculated using DFT as well as obtained through Eq. 5 are shown in Table 5 and they are very similar. Figure S4 (in supporting information) shows graphically the linear fit between experimental $\delta^1$H and calculated $\sigma^1$H for all furan derivatives.

**Table 6** Hammett coefficients for $^1$H-SIS

| | | α | 3 | 4 | 5 |
|---|---|---|---|---|---|
| Trans-SF OC-syn | *a* | 25.0 | 25.6 | 25.5 | 24.5 |
| | *b* | −0.3 | −0.2 | −0.1 | −0.1 |
| | *R* | 0.85 | 0.97 | 0.96 | 0.96 |
| Trans-SF OC-anti | *a* | 24.8 | 25.1 | 25.4 | 24.6 |
| | *b* | −0.3 | −0.2 | −0.1 | −0.1 |
| | *R* | 0.88 | 0.96 | 0.96 | 0.97 |
| Protonated FA ON-syn | *a* | 23.8 | 24.0 | 24.6 | 23.5 |
| | *b* | 0.2 | −0.3 | −0.2 | −0.2 |
| | *R* | 0.86 | 0.78 | 0.87 | 0.83 |
| Protonated FA ON-anti | *a* | 23.5 | 23.9 | 24.5 | 23.5 |
| | *b* | 0.1 | −0.3 | −0.2 | −0.2 |
| | *R* | 0.76 | 0.73 | 0.86 | 0.85 |
| Neutral FA ON-syn | *a* | 23.8 | 25.2 | 25.4 | 24.3 |
| | *b* | −0.1 | −0.2 | −0.1 | −0.1 |
| | *R* | −0.04 | 0.97 | 0.95 | 0.96 |
| Neutral FA ON-anti | *a* | 23.5 | 24.5 | 25.3 | 24.4 |
| | *b* | −0.1 | −0.2 | −0.1 | −0.1 |
| | *R* | 0.02 | 0.96 | 0.95 | 0.97 |

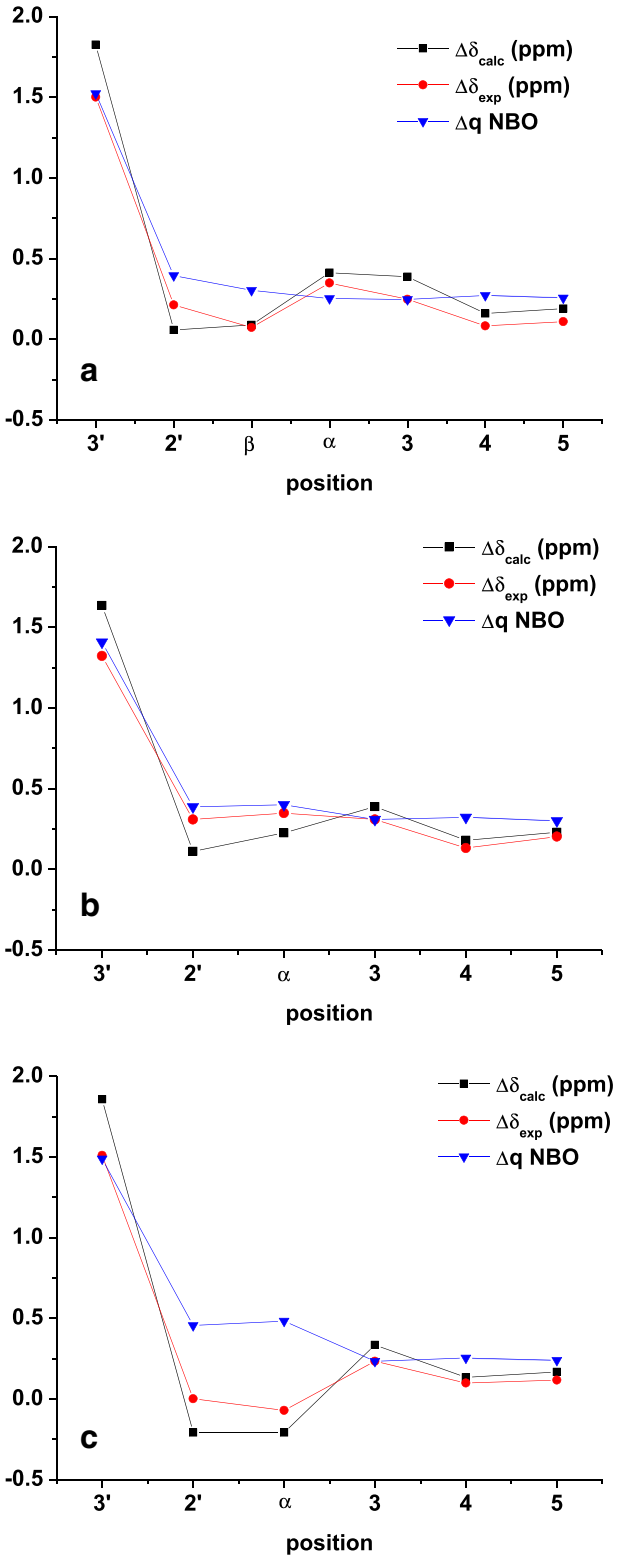


**Fig. 4** $^1$H SIS transmission for (**a**) trans-SF OC-syn (**b**) protonated FA ON-syn and (**c**) neutral FA ON-syn. The $\Delta q$ were calibrated to $\Delta\delta_{exp}$ of position 3

Calculated $\sigma^1$H using DFT for all furan derivatives are listed in Tables S11–S16.

As expected, substituents in 4′ affect in a similar way both $\sigma^1$H and $\sigma^{13}$C when those hydrogen and carbon atoms are bonded directly. In order to estimate the influence of the substituent electronic effect over $\sigma^1$H, we re-define the Hammett equation, Eq. 6, where every term keeps the same meaning than in Eq. 3. Table 6 shows the values of *a*, *b* and *R*, obtained from Eq. 6 for trans-SF and neutral/protonated FA.

$$\sigma^1\mathrm{H(ppm)} = a + b{\cdot}\sigma_p(-\mathrm{X}) \tag{6}$$

$^1$H-SIS can be explained in terms of substituents electronic effects. Therefore, it is possible to define the order in which substituents in 4′ affect $^1$H-SIS in trans SF and neutral/protonated FA as:

$$|b_\alpha| > |b_3| > |b_5| > |b_4|.$$

According to Table 6, all $^1$H–SIS except those of position α in neutral FA, correlate with Hammett constants. $^1$H–SIS of trans SF are the most sensitive to the electronic effect of substituent in 4′. The SIS of $H_\alpha$ in neutral FA shows an anomalous behavior and do not correlate with Hammett constants. A plausible interpretation of the absence of correlation of $H_\alpha$ in neutral FA is the variable relative orientation of ring B, which is analyzed below.

The origin of the previous anomaly can be explained through the modeling of $^1$H–SIS using $\Delta\delta_{exp}{}^1$H, $\Delta\sigma_{calc}{}^1$H and $\Delta q$ (if the anisotropic term is absent and the solvent effects are disregarded). Accordingly, Fig. 4 shows that experimental trends in $^1$H–SISs are fairly well reproduced by the calculated chemical shifts and NBO charge variations. Nevertheless, the fit of $\Delta\sigma^1$H and $\Delta q$ to $\Delta\delta^1$H in Fig. 4 is less satisfactory than the fit of $^{13}$C-SIS in Fig. 3 due to the solvent effect, mainly in protonated FA, not taken into account in the calculations, which affects relatively more $^1$H than $^{13}$C shieldings.

It is noteworthy that $\Delta q$ model fails to reproduce the experimental SIS of $H_\alpha$ in neutral FA derivatives even at the qualitative level, Fig. 4(c) (for similar behavior of the ON-anti conformers see Fig. S7). This result strongly suggests the important role played by the substituent dependent relative orientation of ring B with respect to $H_\alpha$ (anisotropic term) over the $^1$H–SISs values in neutral FA derivatives, which is associated to the different Ψ dihedral angle of the equilibrium geometry found in every derivative. Consequently, the magnetic anisotropic term of ring B affects $^1H_\alpha$–SIS in a trend that opposes the local charge effects.

This variable effect of ring B over $^1H_\alpha$–SIS is overcame after protonation of neutral FA derivatives. In this manner, as protonated FA (as well as trans-SF) derivatives are fairly planar compounds without variable anisotropic term, their $^1H_\alpha$–SIS can behave normally, Fig. 4(a) and (b). Consequently, for protonated FA (and trans-SF) derivatives both theoretical models ($\Delta\sigma^1$H and $\Delta q$) reproduce adequately the experimental results.

## Conclusions

DFT calculations support experimental evidence regarding the shape and height of the rotational barriers and Ψ dihedral angle of the equilibrium geometry in the studied furan derivatives. The barrier and Ψ angle for the equilibrium geometry depend strongly on electronic effect of 4′-substituent for neutral FA. Conversely, these properties are not sensitive to 4′-substituent for trans-SF and protonated FA.

The rotational barrier of neutral FA derivatives can be explained satisfactorily as a sum of local electronic contributions according to NBO methodology. Azomethine N lone pair disponibility for conjugating with B ring π-system accounts for the difference in rotational barrier heights through Ψ=90°.

In contrast, AIM offers an alternative explanation for the instability of the planar conformations in neutral FA. This approach provides a different interpretation opposed to the traditional repulsive interaction between hydrogens.

$^{13}$C and $^1$H isotropic shielding constants of all furan derivatives are well reproduced by DFT calculations. Furthermore, the trends of both types of shieldings are adequately explained by NBO charges. However, $\delta^1H_\alpha$ does not correlate with NBO charge differences due to the variable anisotropic effect of B ring in neutral FA, but is well reproduced by calculated $\sigma^1H_\alpha$.

## References


1. Kaupp M, Buhl M, Malkin V (2004) Calculation of NMR and EPR parameters. Wiley-VHC, Weinheim
2. Vaara J (2007) Theory and computation of nuclear magnetic resonance parameters. Phys Chem Chem Phys 9:5399–5418. doi:10.1039/b706135h
3. Krivdin LB, Contreras RH (2007) Recent advances in theoretical calculations of indirect spin-spin coupling constants. Annu Rep NMR Spectrosc 61:133–245. doi:10.1016/S0066-4103(07)61103-X
4. Casabianca LB, de Dios AC (2008) Ab initio calculations of NMR chemical shifts. J Chem Phys 128:052201. doi:10.1063/1.2816784
5. Helgaker T, Jaszuński M, Pecul M (2008) The quantum-chemical calculation of NMR indirect spin-spin coupling constants. Prog Nucl Magn Reson Spectrosc 53:249–268. doi:10.1016/j.pnmrs.2008.02.002

6. Buhl M (2008) Chapter 3 DFT computations of transition-metal chemical shifts. Annu Rep NMR Spectrosc 64:77–126. doi:10.1016/S0066-4103(08)00003-3
7. Mulder FAA, Filatov M (2010) NMR chemical shift data and ab initio shielding calculations: emerging tools for protein structure determination. Chem Soc Rev 39:578–590. doi:10.1039/b811366c
8. Saitô H, Ando I, Ramamoorthy A (2010) Chemical shift tensor—the heart of NMR: insights into biological aspects of proteins. Prog Nucl Magn Reson Spectrosc 57:181–228. doi:10.1016/j.pnmrs.2010.04.005
9. Facelli JC (2011) Chemical shift tensors: theory and application to molecular structural problems. Prog Nucl Magn Reson Spectrosc 58:176–201. doi:10.1016/j.pnmrs.2010.10.003
10. Bühl M, van Mourik T (2011) NMR spectroscopy: quantum-chemical calculations. WIREs Comput Mol Sci 1:634–647. doi:10.1002/wcms.63
11. Wishart DS (2011) Interpreting protein chemical shift data. Prog Nucl Magn Reson Spectrosc 58:62–87. doi:10.1016/j.pnmrs.2010.07.004
12. Helgaker T, Jaszuński M, Ruud K (1999) Ab initio methods for the calculation of NMR shielding and indirect spin-spin Coupling Constants. Chem Rev 99:293–352. doi:10.1021/cr960017t
13. Pérez C, Suardíaz R, Ortiz PJ et al (2008) On the unusual $^{2}J_{C2-Hf}$ coupling dependence on syn/anti CHO conformation in 5-X-furan-2-carboxaldehydes. Magn Reson Chem 46:846–850. doi:10.1002/mrc.2268
14. Contreras RH, Suardíaz R, Pérez C et al (2008) Karplus equation for $^{3}J_{HH}$ spin-spin couplings with unusual 3J (180°)<$^{3}$J (0°) relationship. J Chem Theory Comput 4:1494–1500. doi:10.1021/ct800145h
15. Saielli G, Bagno A (2009) Can two molecules have the same NMR spectrum? Hexacyclinol revisited. Org Lett 11:1409–1412. doi:10.1021/ol900164a
16. Suardíaz R, Maestre M, Suárez E et al (2008) Molecular dynamics and NMR analysis of the configurational $^{13}$C assignment of epimeric 22,23-epoxides of stigmasterol. J Phys Chem A 112:8333–8336. doi:10.1021/jp804570g
17. Smith SG, Goodman JM (2010) Assigning stereochemistry to single diastereoisomers by GIAO NMR calculation: the DP4 probability. J Am Chem Soc 132:12946–12959. doi:10.1021/ja105035r
18. Contreras RH, Suardíaz R, Pérez C et al (2010) NMR spin-spin coupling constants and hyperconjugative interactions. Int J Quantum Chem 110:532–539. doi:10.1002/qua.22136
19. Bühl M, Wrackmeyer B (2010) Density-functional computation of $^{93}$Nb NMR chemical shifts. Magn Reson Chem 48(Suppl 1):S61–S68. doi:10.1002/mrc.2624
20. Bagno A, Bini R (2010) NMR spectra of terminal oxo gold and platinum complexes: relativistic DFT predictions. Angew Chem, Int Ed Engl 49:1083–1086. doi:10.1002/anie.200905507
21. Suardíaz R, Pérez C, García de la Vega JM et al (2007) Theoretical Karplus relationships for vicinal coupling constants around $\chi_1$ in Valine. Chem Phys Lett 442:119–123. doi:10.1016/j.cplett.2007.05.049
22. Suardíaz R, Crespo-Otero R, Pérez C et al (2011) Communication: accurate determination of side-chain torsion angle $\chi_1$ in proteins: phenylalanine residues. J Chem Phys 134:061101. doi:10.1063/1.3553204
23. Suardíaz R, Sahakyan AB, Vendruscolo M (2013) A geometrical parametrization of C1′-C5′ RNA ribose chemical shifts calculated by density functional theory. J Chem Phys 139:034101. doi:10.1063/1.4811498
24. García De La Vega JM, San Fabián J, Crespo-Otero R et al (2013) Theoretical DFT Karplus equations: amino acid side-chain torsion angle $\chi_1$. Int J Quantum Chem 113:656–660. doi:10.1002/qua.24030
25. Webber AL, Emsley L, Claramunt RM, Brown SP (2010) NMR crystallography of campho[2,3-c]pyrazole (Z′=6): combining high-resolution $^{1}$H-$^{13}$C solid-state MAS NMR spectroscopy and GIPAW chemical-shift calculations. J Phys Chem A 114:10435–10442. doi:10.1021/jp104901j
26. Cuny J, Messaoudi S, Alonzo V et al (2008) DFT calculations of quadrupolar solid-state NMR properties: Some examples in solid-state inorganic chemistry. J Comput Chem 29:2279–2287. doi:10.1002/jcc.21028
27. Griffin JM, Yates JR, Berry AJ et al (2010) High-resolution $^{19}$F MAS NMR spectroscopy: structural disorder and unusual J couplings in a fluorinated hydroxy-silicate. J Am Chem Soc 132:15651–15660. doi:10.1021/ja105347q
28. Salager E, Day GM, Stein RS et al (2010) Powder crystallography by combined crystal structure prediction and high-resolution $^{1}$H solid-state NMR spectroscopy. J Am Chem Soc 132:2564–2566. doi:10.1021/ja909449k
29. Yates JR (2010) Prediction of NMR J-coupling in solids with the planewave pseudopotential approach. Magn Reson Chem 48(Suppl 1):S23–S31. doi:10.1002/mrc.2646
30. Hollenstein R (1985) H.-O. Kalinowski, S. Berger and S. Braun. $^{13}$C NMR-Spektroskopie. Georg Thieme Verlag, Stuttgart 1984. pp. 685. DM98. Magn Reson Chem 23:589–589. doi:10.1002/mrc.1260230721
31. Bagno A (2001) Complete prediction of the $^{1}$H NMR spectrum of organic molecules by DFT calculations of chemical shifts and spin-spin coupling constants. Chem A Europ J 7:1652–1661
32. Bagno A, Rastrelli F, Saielli G (2003) Predicting $^{13}$C NMR spectra by DFT calculations. J Phys Chem A 107:9964–9973. doi:10.1021/jp0353284
33. Tähtinen P, Bagno A, Klika KD, Pihlaja K (2003) Modeling NMR parameters by DFT methods as an aid to the conformational analysis of cis-fused 7a(8a)-methyl octa(hexa)hydrocyclopenta[d][1,3]oxazines and [3, 1]benzoxazines. J Am Chem Soc 125:4609–4618. doi:10.1021/ja021237t
34. Robertson JE, Biel JH, Mitchell TF et al (1963) Hypotensives. VI.1 Disubstituted alkylenediamines and related compounds. J Med Chem 6:805–807. doi:10.1021/jm00342a043
35. Jovanović B, Mišić-Vuković M, Marinković A, Vajs V (1999) Effect of substituents on the $^{13}$C chemical shifts of the azomethine carbon atom of N-(phenyl substituted) pyridine-4-aldimines. J Mol Struct 482–483:375–378. doi:10.1016/S0022-2860(98)00860-6
36. Jovanovic B (2002) Effect of substituents on the $^{13}$C chemical shifts of the azomethine carbon atom of N-(phenyl substituted)pyridine-3- and −2-aldimines. J Mol Struct 642:113–118. doi:10.1016/S0022-2860(02)00403-9
37. Kadaba P (1975) Triazolines. 8. Action of diazoalkanes on heterocyclic substituted Schiff-bases. J Heterocycl Chem 12:143–146
38. Kadaba PK (1988) Triazolines. 14. 1,2,3-Triazolines and triazoles. A new class of anticonvulsants. Drug design and structure-activity relationships. J Med Chem 31:196–203. doi:10.1021/jm00396a032
39. Head R, Jones R (1966) The electronic and infrared spectra of N-aryl furfurylidene- and thenylideneimines. Aust J Chem 19:1747–1749. doi:10.1071/CH9661747
40. Devi P, Sandhu JS, Thyagarajan G (1979) Nuclear magnetic resonance study of furan-2-carbaldehyde N-alkylimines. J Heterocycl Chem 16:1073–1074. doi:10.1002/jhet.5570160549
41. Santos D, Suardiaz R, Montero LA, Pérez C (2008) DFT analysis of rotational barriers, $^{1}$H and $^{13}$C NMR chemical shifts in neutral and protonated furfurylidenanilines. J Mol Struct (THEOCHEM) 852:78–82. doi:10.1016/j.theochem.2007.12.014
42. Pérez C (1979) Dissertation. Humboldt Universität, Berlin, Germany
43. Pérez CS, Ortiz PJ (1982) Estabilidad de azometinos furánicos en medios ácidos. Sitio y reversibilidad de la protonación. Rev CENIC Cienc Quim 13:207
44. Olah GA, Kreienbuehl P (1967) Stable carbonium ions.l. Protonated imines. J Am Chem Soc 89:4756–4759. doi:10.1021/ja00994a033
45. Fischer E, Frei Y (1957) Photoisomerization equilibria involving the C=N double bond. J Chem Phys 27:808–809. doi:10.1063/1.1743834

46. Wettermark G, Weinstein J, Sousa J, Dogliotti L (1965) Kinetics of cis-trans isomerization of para-substituted N-benzylideneanilines. J Phys Chem 69:1584–1587. doi:10.1021/j100889a023
47. Kobayashi M, Yoshida M, Minato H (1976) Configuration of the photoisomers of benzylideneanilines. J Org Chem 41:3322–3324. doi:10.1021/jo00882a026
48. Becke AD (1996) Density-functional thermochemistry. IV. A new dynamical correlation functional and implications for exact-exchange mixing. J Chem Phys 104:1040–1046. doi:10.1063/1.470829
49. Lee C, Yang W, Parr RG (1988) Development of the Colle-Salvetti correlation-energy formula into a functional of the electron density. Phys Rev B 37:785–789. doi:10.1103/PhysRevB.37.785
50. Stephens PJ, Devlin FJ, Chabalowski CF, Frisch MJ (1994) Ab initio calculation of vibrational absorption and circular dichroism spectra using density functional force fields. J Phys Chem 98:11623–11627. doi:10.1021/j100096a001
51. Hertwig RH, Koch W (1997) On the parameterization of the local correlation functional. What is Becke-3-LYP? Chem Phys Lett 268:345–351. doi:10.1016/S0009-2614(97)00207-8
52. Wolinski K, Hinton JF, Pulay P (1990) Efficient implementation of the gauge-independent atomic orbital method for NMR chemical shift calculations. J Am Chem Soc 112:8251–8260. doi:10.1021/ja00179a005
53. Glendening ED, Reed AE, Carpenter JE, Weinhold F NBO Version 3.1. (Included in the Gaussian 03 Revision A.1 package of programs)
54. Frisch MJ, Trucos GW, Schlegel HB et al. (2003) Gaussian 03, revision A.1. Gaussian, Inc, Pittsburg
55. Biegler-König FW, Bader RFW, Tang T-H (1982) Calculation of the average properties of atoms in molecules. II. J Comput Chem 3:317–328. doi:10.1002/jcc.540030306
56. Biegler-König F, Schönbohm J (2002) Update of the AIM2000-program for atoms in molecules. J Comput Chem 23:1489–1494. doi:10.1002/jcc.10085
57. Robertson JM, Woodward I (1937) X-Ray analysis of the dibenzyl series. IV. Detailed structure of stilbene. Proc R Soc A 162:568–583. doi:10.1098/rspa.1937.0203
58. Traetteberg M, Frantsen E, Mijlhoff F, Hoekstra A (1975) A gas electron diffraction study of the molecular structure of trans-stilbene. J Mol Struct 26:57–68. doi:10.1016/0022-2860(75)80066-4
59. Akaba R, Tokumaru K, Kobayashi T, Utsunomiya C (1980) Electronic structures and conformations of N-benzylideneanilines. II. Photoelectron spectral study. Bull Chem Soc Jpn 53:2002–2006. doi:10.1246/bcsj.53.2002
60. Akaba R, Tokumaru K, Kobayashi T (1980) Electronic structures and conformations of N-benzylideneanilines. I. Electronic absorption spectral study combined with CNDO/S CI calculations. Bull Chem Soc Jpn 53:1993–2001. doi:10.1246/bcsj.53.1993
61. Skrabal P, Steiger J, Zollinger H (1975) On the planarisation of benzylideneaniline. Helv Chim Acta 58:800–814. doi:10.1002/hlca.19750580318
62. Bernstein J (1981) An ab initio study of the conformational energetics of N-benzylideneaniline. J Chem Phys 75:2346–2353. doi:10.1063/1.442296
63. Reed AE, Curtiss LA, Weinhold F (1988) Intermolecular interactions from a natural bond orbital, donor-acceptor viewpoint. Chem Rev 88:899–926. doi:10.1021/cr00088a005
64. Bader RFW (2006) Pauli repulsions exist only in the eye of the beholder. Chem A Europ J 12:2896–2901. doi:10.1002/chem.200501589
65. Matta CF, Hernández-Trujillo J, Tang T-H, Bader RFW (2003) Hydrogen-hydrogen bonding: a stabilizing interaction in molecules and crystals. Chem A Europ J 9:1940–1951. doi:10.1002/chem.200204626
66. Bader RFW (1990) Atoms in molecules: a quantum theory. Oxford University Press, Oxford
67. Wolstenholme DJ, Cameron TS (2006) Comparative study of weak interactions in molecular crystals: H-H bonds vs hydrogen bonds. J Phys Chem A 110:8970–8978. doi:10.1021/jp061205i
68. Poater J, Solà M, Bickelhaupt FM (2006) Hydrogen-hydrogen bonding in planar biphenyl, predicted by atoms-in-molecules theory, does not exist. Chem A Europ J 12:2889–2895. doi:10.1002/chem.200500850
69. Poater J, Solà M, Bickelhaupt FM (2006) A model of the chemical bond must be rooted in quantum mechanics, provide insight, and possess predictive power. Chem A Europ J 12:2902–2905. doi:10.1002/chem.200600057
70. Dybiec K, Gryff-Keller A (2009) Remarks on GIAO-DFT predictions of $^{13}C$ chemical shifts. Magn Reson Chem 47:63–66. doi:10.1002/mrc.2350
71. McDaniel D, Brown H (1958) An extended table of Hammett substituent constants based on the ionization of substituted benzoic acids. J Org Chem 23:420–427. doi:10.1021/jo01097a026
72. Hansch C, Leo A, Taft RW (1991) A survey of Hammett substituent constants and resonance and field parameters. Chem Rev 91:165–195. doi:10.1021/cr00002a004